Sensors and Materials, Vol. 36, No. 7 (2024) 2803–2811
MYU Tokyo

S & M 3702

Microwave Dielectric Properties of Ge-substituted $Nd(Ti_{0.5}Mo_{0.5})O_4$ Ceramics for Application in Slot Antenna Liquid Sensor

Yih-Chien Chen* and Tse-Lung Lin

Department of Electrical Engineering, Lunghwa University of Science and Technology,
No. 300, Sec.1, Wanshou Rd., Guishan District, Taoyuan City 333326, Taiwan

(Received January 3, 2024; accepted July 11, 2024)

Keywords: liquid sensor, slot antenna, microwave dielectric properties

The microwave dielectric properties of $NdTi_{(0.5-x)}Ge_xMo_{0.5}O_4$ ceramics were examined using densification and X-ray diffraction (XRD) patterns. As x increased from 0 to 0.05, the unit cell volume decreased, indicating that Ge^{4+} ions were incorporated within Ti^{4+} ions. After sintering at 1425 °C for 4 h, $Nd(Ti_{0.49}Ge_{0.01}Mo_{0.5})O_4$ ceramics achieved a maximum relative density of 98.9%. The unloaded quality factor ($Q_u \times f$) of the $NdTi_{0.49}Ge_{0.01}Mo_{0.5}O_4$ ceramic sintered at 1425 °C for 4 h was 33,400 GHz (at 17.6 GHz). Additionally, this ceramic exhibited a dielectric constant (ε_r) of 17.6 and the obtained temperature coefficient of resonant frequency (τ_f) was −30.8 ppm/°C. In addition, this ceramic was used as a substrate for slot antenna liquid sensor application. We demonstrated how to improve the measurement results as well as the methodology for obtaining the results. As the water content in acetone increased from 0 to 100%, the measured resonant frequencies shifted from 2.6 to 2.0 GHz.

1. Introduction

Environmental monitoring sensors are increasingly widely used in industrial manufacturing plants to guarantee worker safety. Liquid material characterization has applications in environmental monitoring. Microwave-based liquid sensors come in a variety of forms; some use nonresonant measurement techniques, while others use resonant techniques.(1) Because of their contemporary and straightforward design, planar microstrip resonators are a type of resonance-based liquid sensor. More precisely, slot antenna liquid sensors on ceramics are highly desirable as monitoring devices in a harsh environment because of their compact size and high unloaded quality factor ($Q_u \times f$).

The high dielectric constant (ε_r), high $Q_u \times f$, and low temperature coefficient of resonant frequency (τ_f) are the three microwave dielectric properties of materials that are taken into consideration while developing slot antenna liquid sensors for use in applications.(2) Compact and downsized designs are possible with high ε_r. The effective dielectric constant (ε_{eff}) of both the liquid being measured and the substrate affects the performance of liquid sensors using slot

*Corresponding author: e-mail: ee049@mail.lhu.edu.tw
https://doi.org/10.18494/SAM4881

ISSN 0914-4935

antennas. The moderate-ε_r material in a liquid sensor slot antenna is replaced with the high-ε_r material. $Q_u \times f$ is equivalent to the slot antenna's dielectric loss.

Liquid sensors can have losses due to a variety of factors, such as radiation, conduction, and dielectricity.(3) Dielectric and conduction losses adversely affect the frequency and quality factor ($Q \times f$), and thus lower the efficiency of a wireless liquid sensor. Conversely, the slot antenna liquid sensor's performance can be enhanced by lowering radiation. These losses may also have an impact on the wireless liquid sensor's read range and transmission capacity. Additionally, τ_f must be kept small to minimize the impact of harsh environmental conditions on the sensor.(4)

Common solid-state reaction techniques are used to create rare-earth niobate ceramics ($RENbO_4$), which may be applicable in resonators, filters, and antennas in contemporary communications systems.(5) Dielectric constants of 19.3 and 19.6 and $Q_u \times f$ values of 54400 and 33000 GHz were achieved when $LaNbO_4$ and $NdNbO_4$ ceramics, respectively, were sintered for 4 h at a temperature of 1250 °C. The values of τ_f are −9 and −24 ppm/°C, respectively.(6) Ti^{4+} and Mo^{6+} ionic radii are 0.0605 and 0.059 nm, respectively, which are extremely close to the Nb^{5+} ionic radius of 0.064 nm.(7) Because of these similarities, Ti^{4+} and Mo^{6+} ions can take the place of Nb^{5+} ions to create $Nd(Ti_{0.5}Mo_{0.5})O_4$. Furthermore, Ti^{4+} and Mo^{6+} ions have lower dielectric constants than Nb^{5+} ions owing to their poorer ion polarization abilities.(8) This reduces cross-coupling and transmission attenuation. The ionic radius of Ge^{4+} (0.053 nm) is comparable to that of Ti^{4+} (0.0605 nm); hence, we investigated how substituting Ge^{4+} for Ti^{4+} would affect the creation of $NdTi_{(0.5-x)}Ge_xMo_{0.5}O_4$ ceramics.(8) The effects of the Ge substitution level and sintering temperature on the microwave dielectric characteristics of $NdTi_{(0.5-x)}Ge_xMo_{0.5}O_4$ ceramics were investigated. X-ray densification and diffraction (XRD) patterns were used to analyze these various microwave dielectric characteristics.

Because of their excellent efficiency, ease of manufacturing, and compact size, slot antennas are extensively used in cellular and wireless communications, as well as other commercial applications. A half-wavelength slot antenna is usually rectangular.(9) Nevertheless, commercial substrates are not appropriate for use in severe settings owing to their low chemical stability. The antenna in this study has a ceramic substrate structure, which counteracts the negative effects of liquid samples on the antenna. Combining the benefits of a moderate-ε_r microwave ceramic substrate with an affordable slot antenna, a liquid sensor with a slot antenna specifically intended for liquid concentration analysis was developed and tested. Because of its single dielectric substrate and lack of via holes, the suggested slot antenna liquid sensor is simple to construct.

2. Materials and Methods

High-quality raw materials, including MoO_3 powder (99.9%), Nd_2O_3 (99.9%), TiO_2 (99.0%), and GeO_2 (99.99%), are utilized to make the compound $NdTi_{(0.5-x)}Ge_xMo_{0.5}O_4$. The conventional mixed oxide technique is employed to prepare the samples. After stoichiometric weighing, the raw ingredients are mixed and ball-milled in alcohol, dried, and then calcined for 4 h at 1200 °C in air. PVA is utilized as a binder in the reprocessing of calcined powder. After that, the powder is reground using a PVA solution as a binding agent, then put through a 200-mesh sieve. Then, the obtained powder is compressed axially at a pressure of 2000 kg/cm^2 to create pellets that have an 11 mm diameter and a 6 mm thickness. The particles are then sintered in the presence of air at a temperature of 1375 to 1450 °C for 4 h. The whole process maintains a heating and cooling rate of 10 °C/min.

Following sintering, the sample phases were investigated using CuKα radiation set to 30 kV and 20 mA on a Rigaku D/MAX-2200 X-ray diffractometer. A scanning range of 20 to 60° was established for 2θ. The material composition was then ascertained by comparing the X-ray diffraction results with entries in the JCPDS database. Archimedes' method was applied to determine the sample's true density using distilled water as the medium. Next, the difference between the theoretical and apparent densities was used to calculate the relative density (RD).

Hakki and Coleman's(10) post-resonator method was used to assess the microwave dielectric characteristics of the samples. The samples were shaped into a cylinder with specific length and diameter for this test. According to the standards set by Kobayashi and Katoh,(11) the length-to-width ratio (D/L) of these specimens was roughly 1.6. A transmission-type resonator was constructed by placing a cylindrical sample between two parallel metal plates to examine its microwave dielectric properties. Two small antennas were positioned in the best possible way close to the sample in order to guarantee effective coupling to the resonator and improve the efficiency of microwave transmission and reception. The coaxial transmission line's front-end antenna provided the input signal, while the other-end antenna coupled electromagnetic waves that meet the requirements of the resonator. Besides that, an Agilent N5230A network analyzer was connected to the antenna.

The sample size and dielectric properties have an impact on the system's resonant characteristics. Electric field probes were used to couple the microwave energy. To specifically determine the sample loss factor and ε_r, the TE_{011} resonance method was used. Wheless and Kajfez's pattern recognition techniques were used to identify the specific method.(12) The Agilent N5230A network analyzer was utilized to determine the TE_{011} resonant frequency of the dielectric resonator, from which ε_r and $Q_u \times f$ were calculated. The values of τ_f were measured by the same methods. To conduct the experiment, the test cavity was placed within a chamber with temperature control, and the temperature was gradually raised from 25 to 75 °C. τ_f (ppm/°C) was obtained by recording the resonant frequency at each increase of 10 °C and using the following equation:

$$\tau_f = \frac{f_2 - f_1}{f_1 \left(T_2 - T_1\right)}. \tag{1}$$

The resonant frequencies at temperatures T_1 and T_2 are denoted by f_1 and f_2, respectively.

The transmission line shape of the slot was examined to study the liquid sensor of the slot antenna. A commercial electromagnetic simulator was used for the simulations. A 3.5 GHz resonant frequency rectangular slot was used in the design process. Resonance was achieved in the slot antenna by adjusting the nonradiating edge length to half the guided wavelength at 3.5 GHz.(13) The microwave ceramic substrate was polished and ground to the necessary dimensions using grinding and polishing equipment. After that, sandpaper and water were used to polish the substrate on both sides. Then, a 40 min acetone treatment and an ultrasonic vibration cleaning machine were employed to eliminate any leftover material from the polishing stage. Subsequently, deionized water was used to thoroughly wash the substrate to remove any leftover particles or impurities, followed by thorough drying in a regulated space, such as a box with heated air circulation, to guarantee efficient moisture removal. To guarantee total adhesion to the ceramic substrate surface, conductive silver paste was subsequently applied to the substrate surface using a printer and cured at 150 °C for 1 h in the heated air circulation box. Finally, a laser engraving machine and laser ablation were used to complete the slot antenna. A PNA network analyzer (N5230A) was used to calculate the return loss.

3. Results and Discussion

The X-ray diffraction patterns of $Nd(Ti_{0.49}Ge_{0.01}Mo_{0.5})O_4$ sintered at 1375–1450 °C for 4 h are displayed in Fig. 1. The tetragonal $Nd(Ti_{0.5}Mo_{0.5})O_4$ phase (ICDD-PDF 49-0554) is a member of the I41/a(88) space group. A comparison with ICDD-PDF 49-0554 reveals that there is a secondary $Nd_2Ti_2O_7$ phase in addition to the primary $Nd(Ti_{0.5}Mo_{0.5})O_4$ phase, which is shown by a solid circle. The secondary phase persists and the main phase changes little at different sintering temperatures. One possible explanation for the secondary phase could be the excessively high sintering temperature, which would cause molybdenum trioxide to evaporate and produce $Nd_2Ti_2O_7$. The secondary phase may have an impact on the microwave dielectric characteristics of $Nd(Ti_{0.49}Sn_{0.01}Mo_{0.5})O_4$. Ceramics made of $Nd_2Ti_2O_7$ have τ_f of −118 ppm/°C, $Q_u \times f$ of 16,400 GHz, and ε_r of 36. $Nd_2Ti_2O_7$ ceramics have a greater ε_r than $Nd(Ti_{0.49}Ti_{0.01}Mo_{0.5})O_4$ ceramics. On the other hand, $Nd_2Ti_2O_7$ ceramics have a larger negative τ_f, a lower $Q_u \times f$, and

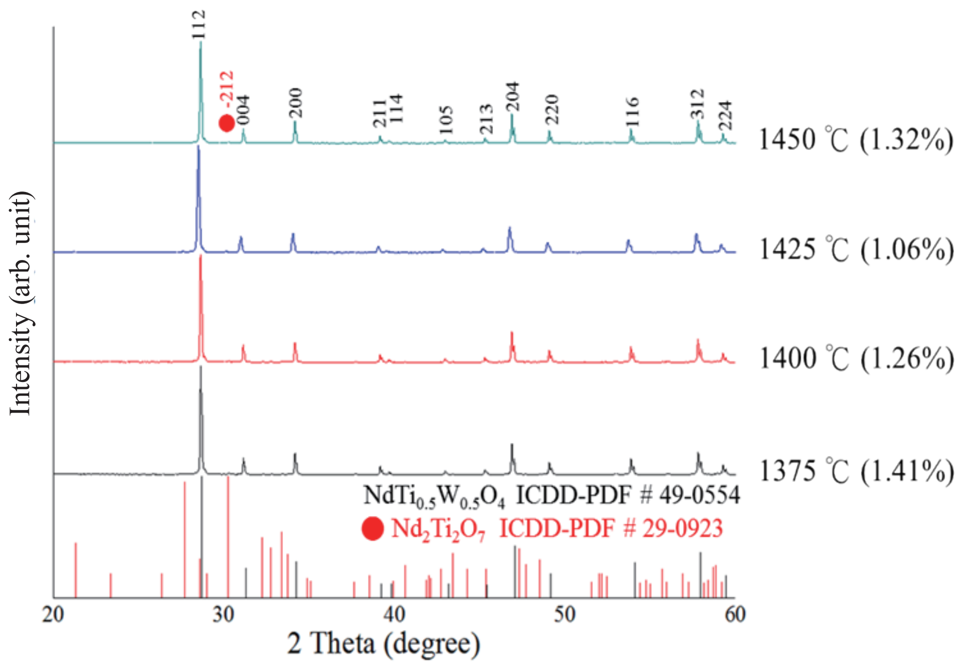

Fig. 1. (Color online) X-ray diffraction patterns of $Nd(Ti_{0.49}Ge_{0.01}Mo_{0.5})O_4$ ceramics sintered for 4 h at 1375–1450 °C.

a greater ε_r than $Nd(Ti_{0.49}Ge_{0.01}Mo_{0.5})O_4$ ceramics. This suggests that the creation of the $Nd_2Ti_2O_7$ phase increased the τ_f, $Q_u \times f$, and ε_r of the sample.(14)

The unit cell volumes of $NdTi_{(0.5-x)}Ge_xMo_{0.5}O_4$ ceramics dropped from 315.3928 to 306.5060 Å³ as x climbed from 0 to 0.05 because Sn^{4+} ions have a smaller ionic radius (0.053 nm) than Ti^{4+} ions (0.0605 nm).(15) The X-ray diffraction patterns allow for the identification of the secondary $Nd_2Ti_2O_7$ ceramic phase at 30.272°. The amount of the secondary $Nd_2Ti_2O_7$ phase is calculated using the intensities of the (1 1 2) diffraction peak of $Nd(Ti_{0.49}Ge_{0.01}Mo_{0.5})O_4$ and the (2 1 1) peak of $Nd_2Ti_2O_7$, and the following equation:

$$NdTi_{0.5}Ge_{0.5}O_4\left(\text{vol\%}\right) = \frac{I_{A(112)}}{I_{A(112)} + I_{B(211)}} \times 100\,. \quad (2)$$

The (1 1 2) diffraction peak of $Nd(Ti_{0.49}Ge_{0.01}Mo_{0.5})O_4$ is represented by I_A in this instance, and the (2 1 1) diffraction peak of $Nd_2Ti_2O_7$ is represented by I_B.

The secondary phase peak intensity in $Nd(Ti_{0.49}Ge_{0.01}Mo_{0.5})O_4$ varied from 1.06 to 1.41% following a 4 h sintering process at temperatures ranging from 1375 to 1450 °C. For the same amount of time, the $NdTi_{(0.5-x)}Ge_xMo_{0.5}O_4$ samples were sintered at 1425 °C, and as x varied from 0 to 0.05, secondary phase peak intensity varied between 1.06 and 1.26%. The small changes in secondary phase peak intensity suggest that increases in substitution amount or sintering temperature have little effect on the sample's microwave dielectric characteristics.(16)

Figures 2 and 3 show the RD and ε_r of the $NdTi_{(0.5-x)}Ge_xMo_{0.5}O_4$ ceramics sintered for 4 h at 1375–1450 °C, respectively. The $NdTi_{(0.5-x)}Ge_xMo_{0.5}O_4$ ceramics had the highest relative density when sintering was completed at 1425 °C after 4 h. The relative density decreased when sintering was completed at a lower temperature. Moreover, the $Nd(Ti_{0.49}Ge_{0.01}Mo_{0.5})O_4$ ceramic had the highest relative density of 98.9% after 4 h of sintering at 1425 °C. ε_r increased from 17.0 to 17.6 as the sintering temperature increased from 1375 to 1425 °C over 4 h. Over the course of 4 h, the sintering temperature increased from 1425 to 1450 °C, causing ε_r to drop from 17.6 to 17.0. The

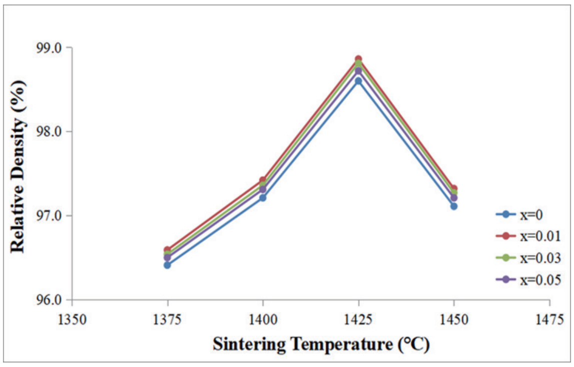

Fig. 2. (Color online) Relative densities of $NdTi_{(0.5-x)}Ge_xMo_{0.5}O_4$ ceramics sintered for 4 h at 1375–1450 °C.

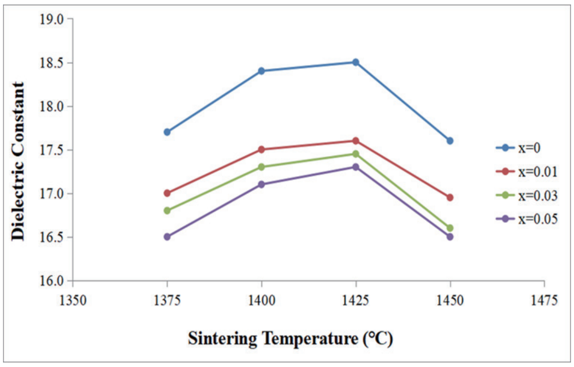

Fig. 3. (Color online) Dielectric constants of $NdTi_{(0.5-x)}Ge_xMo_{0.5}O_4$ ceramics sintered for 4 h at 1375–1450 °C.

link between sintering temperature and relative density had a similar pattern to that between sintering temperature and ε_r. For the $NdTi_{(0.5-x)}Ge_xMo_{0.5}O_4$ ceramics sintered at 1425 °C, ε_r decreased from 18.5 to 17.3. A number of variables, referred to as dependent and extraneous variables, affect ε_r.[17] A typical attribute of an element is its ionic polarizability, while external effects may include relative density and open porosity. The ε_r of $NdTi_{(0.5-x)}Ge_xMo_{0.5}O_4$ ceramics is calculated using the Clausius–Mossotti equation, which shows that molar volume and ionic polarization have an impact on ε_r. The Clausius–Mossotti equation states that a higher ε_r corresponds to either a smaller molar volume or a greater ionic polarization. Ionic polarization has less of an effect on ε_r than molar volume does.

Ti^{4+} and Ge^{4+} ions in this investigation have ionic polarizabilities of 2.93 and 1.63 Å^3, respectively.[18] When x is added to the equation, the overall ionic polarizations of the individual ions in $NdTi_{(0.5-x)}Ge_xMo_{0.5}O_4$ ceramics decrease; therefore, ε_r decreases as x increases.

The $Q_u \times f$ and τ_f of the $NdTi_{(0.5-x)}Ge_xMo_{0.5}O_4$ ceramic sintered at 1375–1450 °C for 4 h are shown in Figs. 4 and 5, respectively. The $NdTi_{(0.5-x)}Ge_xMo_{0.5}O_4$ ceramic sintered for 4 h at 1425 °C exhibited the highest $Q_u \times f$ of 33,400 GHz. Microwave dielectric loss, which includes both intrinsic and extrinsic losses, is affected by a variety of factors. The vibrational modes of the lattice are related to intrinsic loss. Numerous variables, including contaminants, the existence of secondary phases, density, porosity, lattice defects, grain size, and oxygen vacancies, are associated with extrinsic loss.[17,18] The $Q_u \times f$ of $NdTi_{(0.5-x)}Sn_xMo_{0.5}O_4$ ceramics tended to increase with x, suggesting that densification has a major impact on $Q_u \times f$ under strain. The maximum relative density within the $NdTi_{(0.5-x)}Ge_xMo_{0.5}O_4$ ceramics range was 98.9%. Furthermore, the τ_f of the ceramics was observed to depend on the composition and amount of the secondary phase.

Conversely, $NdTi_{(0.5-x)}Ge_xMo_{0.5}O_4$ ceramics exhibited no discernible variation in τ_f over the range of sintering temperatures investigated. The τ_f of $Nd(Ti_{0.49}Ge_{0.01}Mo_{0.5})O_4$ ceramics varied between −30.5 and −30.8 ppm/°C when the sintering temperature changed. The $Nd(Ti_{0.49}Ge_{0.01}Mo_{0.5})O_4$ ceramic sintered at a temperature of 1425 °C for 4 h showed a τ_f value of −30.8 ppm/°C.

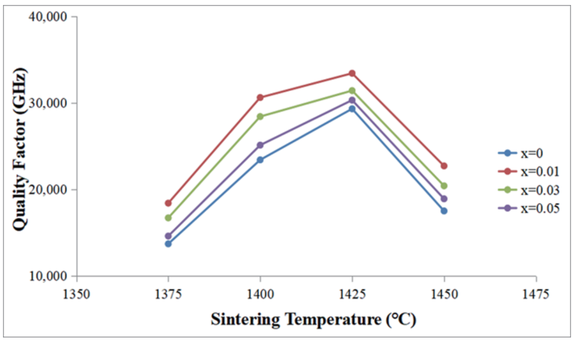

Fig. 4. (Color online) Quality factors of $NdTi_{(0.5-x)}Ge_xMo_{0.5}O_4$ ceramics sintered for 4 h at 1375–1450 °C.

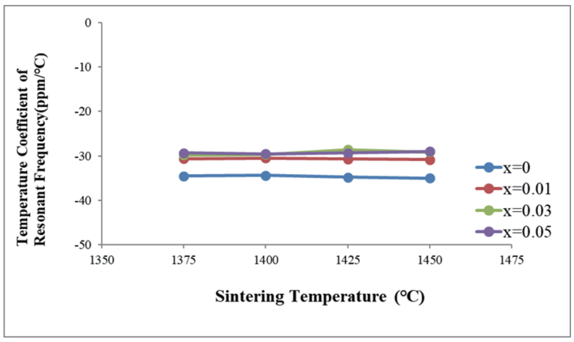

Fig. 5. (Color online) Temperature coefficients of resonant frequency of $NdTi_{(0.5-x)}Ge_xMo_{0.5}O_4$ ceramics sintered for 4 h at 1375–1450 °C.

Figure 6 depicts the slot antenna constructed on a $Nd(Ti_{0.49}Ge_{0.01}Mo_{0.5})O_4$ substrate. For it, a microstrip feed line with a characteristic impedance of 50 Ω is intended. Assuming an infinite ground plane and a finite dielectric density, the dimensions of the microstrip line are calculated using the closed-form methods given in Ref. 19. The size of the microstrip line were confirmed using the AWR Microwave Office. The rectangular slot measures 17.0×2.5 mm^2 in size. Figure 7 shows the simulation and measurement findings of the slot antenna's return loss in air. The modeling and test results of return losses are −30.8 and −18.2 dB, respectively, at 3.45 and 3.40 GHz. The simulated and measured resonant frequencies are close to each other.

The measured return loss of the liquid sensor with a slot antenna with various acetone–water concentrations is shown in Fig. 8. As the water content rises, the resonance frequency of the

Fig. 6. (Color online) Photograph of a liquid sensor prototype with a slot antenna on a Nd(Ti0.49Ge0.01Mo0.5)O4 substrate.

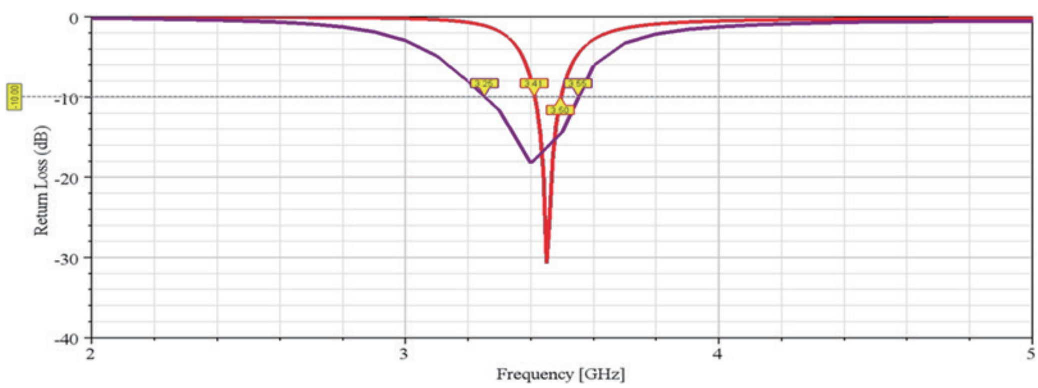

Fig. 7. (Color online) Measured return loss of liquid sensor slot antenna in air.

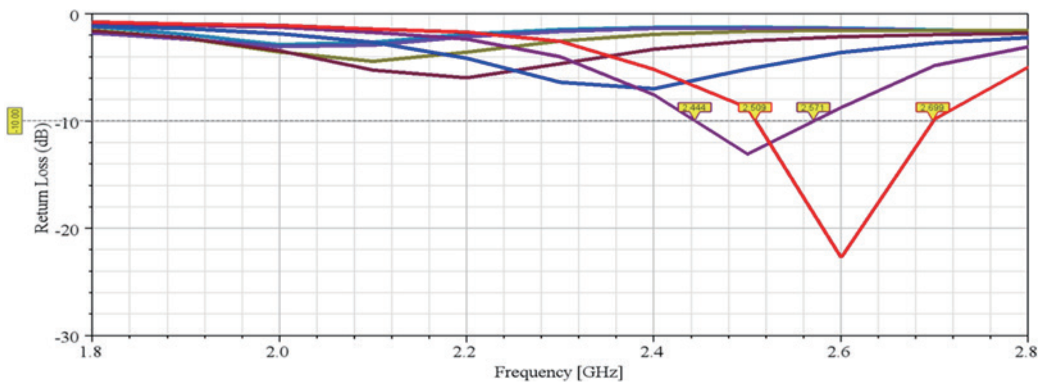

Fig. 8. (Color online) Variation in the measured return loss for the slot antenna liquid sensor with the concentration of water in acetone.

antenna sensor in contact with acetone decreases. This is consistent with the liquid's dielectric characteristics, which fluctuate depending on the ratio of water to acetone, as predicted. The frequency varies in accordance with the permittivity of the liquid, as expected.(20) The resonant frequencies used in the measurement decrease from 2.6 to 2.0 GHz when the concentration of water in acetone increases from 0 to 100%. The resonant frequency decreases almost linearly with increasing percentage of water in acetone. As the concentration of water in acetone increases, there is an increase in matching loss for the slot antenna; this clearly indicates that the return loss decreases with rising water concentration in acetone.

5. Conclusions

The effects of sintering temperature and duration on the dielectric properties of $NdTi_{(0.5-x)}Ge_xMo_{0.5}O_4$ ceramics were investigated. The X-ray diffraction patterns of $Nd(Ti_{0.49}Ge_{0.01}Mo_{0.5})O_4$ ceramics did not change as the sintering temperature increased. The dielectric properties were governed by the sintering temperature. After sintering $Nd(Ti_{0.49}Ge_{0.01}Mo_{0.5})O_4$ ceramics for 4 h at 1425 °C, their τ_f was −30.7 ppm/°C, $Q_u \times f$ was 33400 GHz, and relative density was 98.9%. The proposed liquid sensor with a slot antenna had an easy-to-manufacture structure. Slot antenna liquid sensors are attractive for further development and industrial application because of their high sensitivity, low loss, and resilience.

Acknowledgments

The Ministry of Science and Technology in Taiwan, under Contract No. MOST 111-2221-E-262-001, provided financial assistance for this research, which the authors gratefully acknowledge.

References

1 L. F. Chen, C. Ong, C. Neo, V. Varadan, and V. K. Varadan: Microwave Electronics: Measurement and Materials Characterization (John Wiley & Sons, Chichester, 2004) p. 552.
2 R. D. Shannon: Acta Cryst. **32** (1976) 751. https://doi.org/10.1111/j.1551-2916.2006.01302.x
3 D. M. Pozar: Microwave Engineering (John Wiley, New York, 2011) 4th ed., p. 752.
4 W. L. Stutzman and G. A. Thiele: Antenna Theory and Design (John Wiley & Sons, Hoboken, 2012) 3rd ed., p. 848
5 G. J. McCarthy: Acta Cryst. B**27** (1971) 2285. https://doi.org/10.1107/S0567740871005697
6 D. W. Kim, D. K. Kwon, S. H. Yoon, and K. S. Hong: J. Am. Ceram. Soc. **89** (2006) 3861. https://doi.org/10.1111/j.1551-2916.2006.01302.x
7 Y. C. Chen, M. Z. Weng, Y. X. Du, and C. L. Hsiao: J. Mater. Sci. Mater. Electron. **29** (2018) 4717. https://doi.org/10.1007/s10854-017-8424-y
8 R. D. Shannon: J. Appl. Phys. **73** (1993) 348. https://doi.org/10.1063/1.353856
9 K. Chang, I. Bahl, and V. Nair: RF and Microwave Circuit and Component Design for Wireless Systems (John Wiley & Sons, New York, 2001) 1st ed., p. 532.
10 B. W. Hakki and P. D. Coleman: IRE Trans. Microwave Theory Tech. **8** (1960) 402. https://doi.org/10.1109/TMTT.1960.1124749
11 Y. Kobayashi and M. Katoh: IEEE Trans. Microwave Theory Tech. **85** (1985) 586. https://doi.org/10.1109/TMTT.1985.1133033
12 P. Wheless and D. Kajfez: IEEE MTT-S International Microwave Symposium Digest (IEEE, 1985) 473–476. https://doi.org/10.1109/MWSYM.1985.1132014
13 C. A. Balanis: Antenna theory and design (John Wiley &Sons, Hoboken, 1997) 2nd ed., p. 848.
14 C. Li, X. Wei, H. Yan, and M. J. Reece: J. Eur. Ceram. Soc. **32** (2012) 4015. https://doi.org/10.1016/j.jeurceramsoc.2012.06.002
15 W. S. Kim, T. H. Hong, E. S. Kim, and K. H. Yoon: Jpn. J. Appl. Phys. **37** (1998) 3567. https://doi.org/10.1143/JJAP.37.5367
16 B. D. Silverman: Microwave absorption in cubic strontium titanate. Phys. Rev. **125** (1962) 1921. https://doi.org/10.1103/PhysRev.125.1921
17 Y. Tohdo, K. Kakimoto, H. Ohsato, H. Yamada, and T. Okawa: J. Eur. Ceram. Soc. **26** (2006) 2039. https://doi.org/10.1016/j.jeurceramsoc.2005.09.098
18 C. Veneis, P. K. Davies, T. Negas, and S. Bell: Mater. Res. Bull. **31** (1996) 431. https://doi.org/10.1016/S0025-5408(96)00028-1
19 K. C. Gupta, R. Garg, I. Bahl, and P. Bhartia: Microstrip Lines and Slotlines (Artech House, Boston London, 1996) 2nd ed., p. 560.
20 R. Moolat, M. Mani, and M. Pezholil: Eng. Sci. Technol. Int. J. **32** (2022) 101063. https://doi.org/10.1016/j.jestch.2021.09.009

About the Authors

Yih-Chien Chen received his B.S., M.S., and Ph.D. degrees in electrical engineering from National Cheng Kung University, Tainan, Taiwan, in 1994, 1996, and 2000, respectively. He is currently a distinguished professor in the Department of Electrical Engineering, Lunghwa University of Science and Technology, Taoyuan, Taiwan. His research interests are in microwave engineering, microwave ceramics, and sensors. (ee049@mail.lhu.edu.tw)

Tse-Lung Lin received his B.S. degree in electrical engineering from Lunghwa University of Science and Technology, Taoyuan, Taiwan, in 2021. He is currently an M.S. student in the Department of Electrical Engineering, Lunghwa University of Science and Technology, Taoyuan, Taiwan. His research interests are in microwave engineering, microwave ceramics, and sensors. (88648864a@gmail.com)